Aquaporin-4–dependent K$^+$ and water transport modeled in brain extracellular space following neuroexcitation

Byung-Ju Jin,[1] Hua Zhang,[1] Devin K. Binder,[3] and A.S. Verkman[1,2]

[1]Department of Medicine and [2]Department of Physiology, University of California, San Francisco, San Francisco, CA 94143
[3]Center for Glial-Neuronal Interactions, Division of Biomedical Sciences, University of California, Riverside, Riverside, CA 92521

Potassium (K$^+$) ions released into brain extracellular space (ECS) during neuroexcitation are efficiently taken up by astrocytes. Deletion of astrocyte water channel aquaporin-4 (AQP4) in mice alters neuroexcitation by reducing ECS [K$^+$] accumulation and slowing K$^+$ reuptake. These effects could involve AQP4-dependent: (a) K$^+$ permeability, (b) resting ECS volume, (c) ECS contraction during K$^+$ reuptake, and (d) diffusion-limited water/K$^+$ transport coupling. To investigate the role of these mechanisms, we compared experimental data to predictions of a model of K$^+$ and water uptake into astrocytes after neuronal release of K$^+$ into the ECS. The model computed the kinetics of ECS [K$^+$] and volume, with input parameters including initial ECS volume, astrocyte K$^+$ conductance and water permeability, and diffusion in astrocyte cytoplasm. Numerical methods were developed to compute transport and diffusion for a nonstationary astrocyte–ECS interface. The modeling showed that mechanisms b–d, together, can predict experimentally observed impairment in K$^+$ reuptake from the ECS in AQP4 deficiency, as well as altered K$^+$ accumulation in the ECS after neuroexcitation, provided that astrocyte water permeability is sufficiently reduced in AQP4 deficiency and that solute diffusion in astrocyte cytoplasm is sufficiently low. The modeling thus provides a potential explanation for AQP4-dependent K$^+$/water coupling in the ECS without requiring AQP4-dependent astrocyte K$^+$ permeability. Our model links the physical and ion/water transport properties of brain cells with the dynamics of neuroexcitation, and supports the conclusion that reduced AQP4-dependent water transport is responsible for defective neuroexcitation in AQP4 deficiency.

INTRODUCTION

Astrocytes, a major cell type in the central nervous system (CNS), express the water-selective plasma membrane transporter aquaporin-4 (AQP4; Frigeri et al., 1995; Nielsen et al., 1997). In addition to its well-characterized roles in water balance in brain and spinal cord (Manley et al., 2000; Papadopoulos et al., 2004) and astrocyte migration (Saadoun et al., 2005; Auguste et al., 2007), several lines of evidence implicate the involvement of AQP4 in neuroexcitation (for review see Verkman et al., 2011). Mice lacking AQP4 have prolonged seizure activity after electrical stimulation (Binder et al., 2006) and prolonged cortical spreading depression after mechanical stimulation (Padmawar et al., 2005). Reduced AQP4 expression in human epileptic brain has also been taken as evidence for involvement of AQP4 in neuroexcitation (Eid et al., 2005). As in brain and spinal cord, where AQP4 is expressed in astrocytes adjacent to (non-AQP-expressing) electrically excitable cells (neurons), AQP4 is also expressed in support cells adjacent to excitable cells in neurosensory tissues, including Müller cells (but not bipolar cells) in retina, supportive cells (but not hair cells) in the inner ear, and support cells (but not olfactory receptor neurons) in olfactory epithelium (Takumi et al., 1998; Nagelhus et al., 2004).

AQP4 knockout mice manifest impaired evoked potential responses to light (Li et al., 2002), sound (Li and Verkman, 2001), and olfactory stimuli (Lu et al., 2008).

Studies in brain in vivo and in brain slices of AQP4-deficient mice show slowed accumulation of potassium (K$^+$) in brain extracellular space (ECS) during neuroexcitation (Binder et al., 2006; Strohschein et al., 2011), and slowed clearance of K$^+$ from the ECS after neuroexcitation (Padmawar et al., 2005; Strohschein et al., 2011). Altered ECS K$^+$ dynamics are thought to account for the neuroexcitation phenotype; for example, slowed K$^+$ clearance would prolong seizure duration, as has been found experimentally (Binder et al., 2006). As diagrammed in Fig. 1 A, the ECS is the confined aqueous compartment between brain cells, representing ∼20% of total brain volume (Fenstermacher and Kaye, 1988; Nicholson and Syková, 1998). K$^+$ is released into the ECS by neurons in response to membrane depolarization during neuroexcitation, and cleared mainly by uptake in astrocytes to reestablish the preexcitation state. K$^+$ reuptake is mediated by the inwardly rectifying K$^+$ channel, Kir4.1, and other astrocyte K$^+$ transporters

(Walz and Hertz, 1983; Walz and Hinks, 1985; Ballanyi et al., 1987; Bay and Butt, 2012), and is accompanied by an up to ~30% reduction in ECS volume (Dietzel et al., 1982; Grisar, 1984; Ransom et al., 1985). The principal determinants of K^+ uptake after neuroexcitation include the electrochemical driving force, astrocyte K^+ permeability, ECS volume, and, by unclear mechanisms, AQP4 water permeability. Astrocyte water permeability is greatly reduced in AQP4 deficiency (Solenov et al., 2004).

The mechanistic link between K^+ uptake by astrocytes and AQP4 water permeability has been unclear. One widely speculated possibility, a functional interaction between AQP4 and Kir4.1 (Nagelhus et al., 1999), was not supported by patch-clamp analysis of freshly isolated brain astrocytes (Zhang and Verkman, 2008) and retinal Müller cells (Ruiz-Ederra et al., 2007), as well as brain slices (Strohschein et al., 2011), each showing that AQP4 expression did not affect Kir4.1 K^+ channel function. As discovered originally by cortical surface photobleaching (Binder et al., 2004) and microfiberoptic photobleaching (Zador et al., 2008) measurements of fluorescent dye diffusion in brain ECS in vivo, AQP4 deficiency is associated with mild, chronic ECS expansion. Quantitative ECS volume measurements by triethylammonium iontophoresis (Yao et al., 2008) and fluorescent dye partitioning (Zhang and Verkman, 2010) indicated ~20% greater brain ECS volume in AQP4 knockout mice than in wild-type mice. Whether mild ECS expansion could account for the altered ECS K^+ dynamics in AQP4 deficiency is unclear. Alternative speculative, but untested, possibilities to link astrocyte AQP4 water permeability to K^+ uptake include coupling of K^+ and water transport through changes in ECS volume, or through diffusion-limited transport ("pseudo-solvent drag"; Walz and Hertz, 1983, 1985). For example, K^+ uptake by astrocytes drives osmotic water influx and consequent ECS shrinkage, which would partially maintain the electrochemical driving force for K^+ reuptake and hence potentially account for slowed K^+ reuptake from the ECS in AQP4 deficiency.

We investigated here, by modeling, the role of the various possible mechanisms to account for AQP4-dependent K^+ accumulation into and reuptake from the ECS with neuroexcitation. The hypothesis was tested as to whether reduced AQP4 water permeability in AQP4 deficiency could, by itself, account for the altered ECS K^+ dynamics, and, if so, by how much would astrocyte water permeability need to be reduced in AQP4 deficiency, and how low would solute diffusion need to be in the astrocyte cytoplasm. As diagrammed in Fig. 1 B, the model consists of an ECS layer in contact with neuron
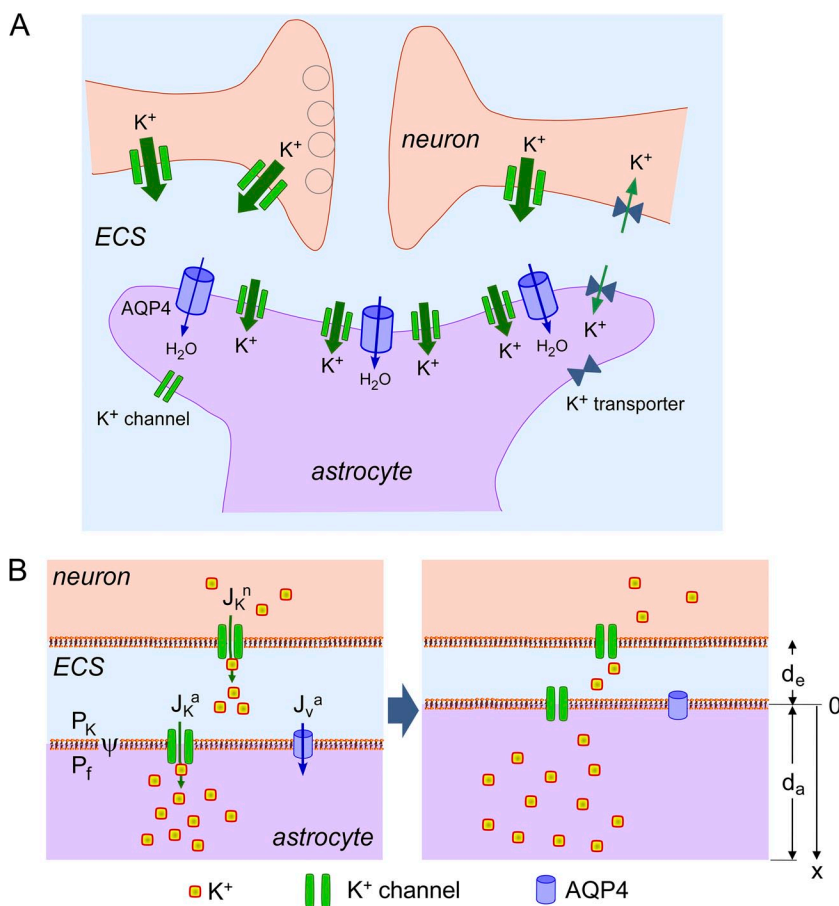
Figure 1. Model of K^+ and water transport in brain ECS. (A) Diagram showing neurons and astrocytes in brain surrounded by an ECS. (B) Schematic of mathematical model. Neuronal, ECS, and astrocytic compartments are shown, along with key transport mechanisms including neuronal K^+ release (J_K^n), K^+ uptake by astrocytes (J_K^a), and osmotic water transport into astrocytes (J_V^a).

and astrocyte layers, in which K^+ is released into the ECS from neurons and taken up by astrocytes. Model specifications include the duration and magnitude of neuronal K^+ release, initial volume, and K^+ concentration in ECS and astrocyte compartments, astrocyte K^+ and water permeability, and diffusion in astrocyte cytoplasm. Model predictions include the kinetics of ECS volume and $[K^+]$ after neuroexcitation, as well as astrocyte water and K^+ fluxes, membrane potential, and cytoplasmic diffusion profiles. A unique aspect and technical challenge in our model was the computation of diffusion-limited transport for a nonstationary astrocyte–ECS interface.

Our model builds on the recent work of Østby et al. (2009), who modeled ECS volume in response to various gene deletions. In contrast to the model of Østby et al. (2009), our model included diffusion-limited solute transport, and, whereas Østby et al. (2009) explicitly included Na^+, K^+, Cl^-, and HCO_3^-, and their multiple associated transporters, our model was formulated to focus on K^+ and water transport with a minimal parameter set. Our model here also builds on the ideas of Chen and Nicholson (2000), who introduced the concept of diffusion-limited solute transport in the ECS, though water permeability or diffusion-limited solute transport in astrocyte cytoplasm were not considered. The inclusion of diffusion-limited solute transport and astrocyte water permeability in our model were crucial to account for experimental data on the influence of AQP4 deficiency on ECS K^+ dynamics. Our model does not take into account spatial buffering, as it focuses on a single neuron–glia–ECS unit and its momentary responses. Thus, details of three-dimensional tissue structure and gap junctions between astrocytes are not taken into account explicitly, nor are K^+ spatial buffering accomplished by astrocytic networks, or the contribution of blood vessel K^+ recycling.

MATERIALS AND METHODS

Model parameters
Constant parameters:
P_f, astrocyte water permeability (cm/s)
P_K, astrocyte K^+ permeability (cm/s)
v_W, partial molar volume of water (18 cm^3/mol)
D_a, diffusion coefficient in astrocyte cytoplasm (cm^2/s)
Δt, computation time step (s)

Variable parameters:
$d_a(t)$, astrocyte volume (layer thickness, μm)
$d_e(t)$, ECS volume (layer thickness, μm)
x, location in astrocyte cytoplasm (distance from the plasma membrane, μm)
$[K^+]_e(t)$, ECS K^+ concentration (mM)
$[K^+]_a(x,t)$, astrocyte K^+ concentration (mM)
$[non-K^+]_a(x,t)$, astrocyte non-K^+ solute concentration (mM)
$J_K^a(t)$, K^+ flux from astrocyte to ECS (mol/cm^2/s)
$J_K^n(t)$, K^+ flux from neuron to ECS (mol/cm^2/s)
$J_K^{a}{}_{pump}(t)$, K^+ flux from astrocyte to ECS by K^+ pump (mol/cm^2/s)

$J_V^a(t)$, water flux from astrocyte to ECS (mol/cm^2/s)
$\psi(t)$, astrocyte plasma membrane potential (mV)
$\Phi_e(t)$, ECS osmolarity (mosM)
$\Phi_a(x,t)$, astrocyte osmolarity (mosM)
δ, buffer region length (μm)

Model computations
As diagrammed in Fig. 2, model computations involve input of parameters and starting values, followed by computation of membrane potential, K^+ and water fluxes, and ECS and astrocyte volumes. Concentrations of K^+ and non-K^+ solutes, and osmolalities, are computed at time $t + \Delta t$, with instantaneous mixing in the well-mixed model or diffusion-limited mixing in the diffusion-limited model, the latter requiring numerical solution of the diffusion equation to generate spatial concentration profiles. At each time step, outputted parameters include concentrations, fluxes, membrane potential, and volumes.

Astrocyte membrane potential $\psi(t)$ is computed from the Nernst-Planck equation (Eq. 1 in Table 1) in which parameters α (340.7 mM) and β (14.0 mM) describe effects of non-K^+ ions (mainly Cl^-), such that $\psi(0) = -83$ mV for $[K^+]_e(0) = 5$ mM and $[K^+]_a(0) = 140$ mM, and $\psi = -77$ mV when $[K^+]_e$ increases from 5 to 10 mM after neuronal excitation, based on experimental data (Chow et al., 1991). K^+ efflux from neurons into the ECS (neuroexcitation) is specified by $J_K^n(t)$, which was generally taken as a step function ($J_K^n(t) = J_K^o$ for $t_1 < t < t_2$ and 0 for $t < t_1$ and $t > t_2$).

K^+ flux between the ECS and astrocyte is determined by the electrochemical driving force as described by the Goldman-Hodgkin-Katz flux (Eq. 2), in which a pump term ($J_K^{a}{}_{pump}$) is included (corresponding to Na^+/K^+ ATPase) to balance resting K^+ leak to give $J_K^a(0) = 0$. $J_K^{a}{}_{pump}$ in Eq. 3 is a saturable function of astrocyte-to-ECS K^+ gradient ($\Delta[K^+]$) and has $\sim$50% of maximal activity under resting conditions (Grisar, 1984; Odette and Newman, 1988). $J_K^{a}{}_{pump}(0)$ is the pump activity under resting conditions that gives zero net K^+ flux ($J_K^a(0) = 0$) by balancing conductive K^+
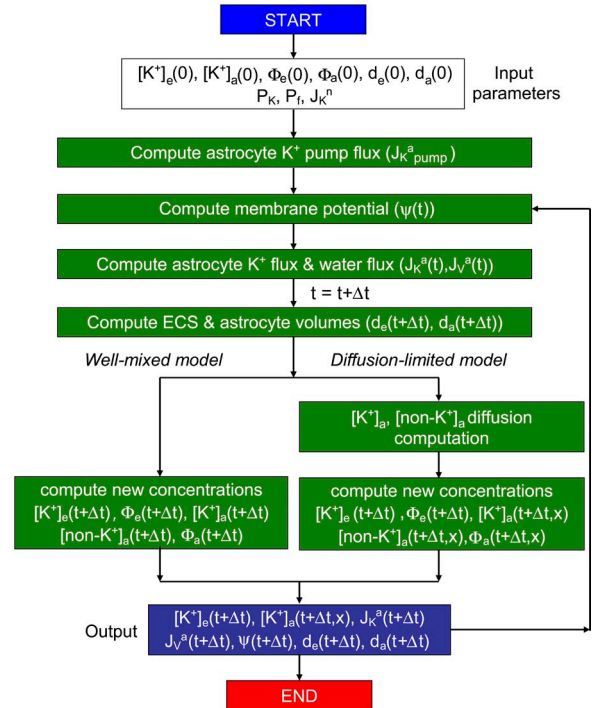
Figure 2. Computational approach. See the Model computations section for description.

leak from astrocytes at the resting potential. To minimize model parameters, we do not include a separate pump term for ECS K+ reuptake into neurons.

The osmotically induced volume flux from the ECS to astrocyte compartments is given by Eq. 4. After volume flux, the new ECS and astrocyte volumes are given by Eqs. 5 and 6, where the ECS volume change is determined by volume flux from the ECS to the astrocyte. The new concentrations of K+ are given by Eqs. 7 and 8, which represent the concentration change resulting from water flux and the amount of K+ flux. Table S1 provides the discretized equivalents of the differential and integral equations as used for numerical solution. Φ_e and Φ_a are given as integral Eqs. 9 and 10. The concentration of non-K+ solutes in astrocyte cytoplasm is computed by Eq. 11, where the factor of 2 has been included for electroneutrality (as Cl− is implicit in the model). Modeling effects of inclusion of electroneutral K+ transport, and effects of factors other than 2, are reported in the supplemental text. The equations above assume that K+ and non-K+ solutes are well-mixed in the astrocyte compartment (well-mixed model).

In the diffusion-limited model, diffusion of K+ and non-K+ solutes in cytoplasm is described by Eqs. 12 and 13, in which diffusion coefficient D_a is assumed to be equal for K+ and non-K+ solutes, which simplifies the description of electrochemical diffusion (Truc et al., 2000). The diffusion equation was solved numerically by the Crank-Nicolson method involving spatial discretization (details in the supplemental text). A flux boundary condition was applied at the plasma membrane (Eq. 14), with zero K+ flux at the opposite membrane. Because the astrocyte–ECS boundary is nonstationary because of water flux, new mesh elements were added at the expanded boundary and a nonuniform mesh was used. The minimum mesh size was 1.5 nm, much less than astrocyte thickness of 10 µm, and the computational time step was generally 10^{-5} s.

In alternative variations of the model (see supplemental text), electroneutral K+ uptake by astrocytes was considered, as well as nonuniform ECS geometry. Model accuracy was confirmed from the insensitivity of computed $[K^+]_e(t)$, $[K^+]_a(t)$, and $d_e(t)$ to time-step size, and, for the diffusion-limited model, from insensitivity of $[K^+]_a(x,t)$ to mesh-element size, and from agreement with analytical solutions to Eqs. 12 and 13 (Table S1; see supplemental text).

Code for the modeling here was written in Visual Fortran (f90 compiler, Microsoft Visual Studio 2008).

Online supplemental material

Contents include additional details of mathematical modeling, including the discretization methodology and other details pertaining to diffusion computations for the moving boundary problem, as well as validation computations and description of alternative model variations. The online supplemental material is available at http://www.jgp.org/cgi/content/full/jgp.201210883/DC1.

RESULTS

Model overview

To focus on the central issue of K+/water transport coupling in the ECS, the model was formulated with minimal assumptions about ECS geometry, K+ transport mechanisms, and input parameters. The model comprises planar neuron, ECS, and astrocyte layers (Fig. 1 B). The location of the neuron–ECS interface was fixed, with neuroexcitation modeled as isosmolar release of K+ into the ECS by neurons (equivalent of K+/Na+ exchange), with magnitude and kinetics specified from experimental data (Grisar, 1984; Sick et al., 1987). Reuptake of K+ from the ECS occurs by transport into astrocytes, as determined by the electrochemical driving force (ECS and astrocyte [K+], and membrane potential) and astrocyte K+ conductance, as specified from experimental data (Walz and Hertz, 1983; Zhang and

TABLE 1
Model equations

| Equation type	Equation	Equation number
Membrane potential equation		
Membrane potential	$\psi = (RT/F) \ln[(\alpha + [K^+]_e)/(\beta + [K^+]_a)]$	1
Flux equations		
Potassium flux	$J_K{}^a = P_K(\psi F/RT)([K^+]_a - [K^+]_e \exp(-\psi F/RT))/(1 - \exp(-\psi F/RT)) - J_K{}^a{}_{pump}$	2
Potassium pump flux	$J_K{}^a{}_{pump} = 2J_K{}^a{}_{pump}(0) [1 + [K^+]_e(0)/(\Delta[K^+] - \Delta[K^+](0) - 2[K^+]_e(0))]$	3
Water flux	$J_V{}^a = P_f v_W(\Phi_e - \Phi_a)$	4
Differential equations for volume and concentration		
ECS volume	$d(d_e)/dt = J_V{}^a$	5
Astrocyte volume	$d(d_a)/dt = -J_V{}^a$	6
ECS [K+]	$d[K^+]_e/dt + (J_V{}^a/d_e)[K^+] = J_K{}^a/d_e$	7
Astrocyte [K+]	$d[K^+]_a/dt - (J_V{}^a/d_a)[K^+] = -J_K{}^a/d_a$	8
Integral equations for osmolarity		
ECS osmolarity	$\Phi_e = \Phi_e(0)/d_e + 2(\int J_K{}^a dt)/d_e$	9
Astrocyte osmolarity	$\Phi_a = \Phi_a(0)/d_a - 2(\int J_K{}^a dt)/d_a$	10
Non-K+ osmolarity	$[non-K^+]_a = \Phi_a(t + \Delta t) - 2[K^+]_a$	11
Diffusion equations		
K+ diffusion	$\partial[K^+]/\partial t = D_a \partial^2[K^+]/\partial x^2$	12
Non-K+ diffusion	$\partial[non-K^+]/\partial t = D_a \partial^2[non-K^+]/\partial x^2$	13
Equation for flux through the moving membrane		
Flux boundary condition	$\partial[K^+]_a/\partial t = -J_K{}^a /\delta$	14

Verkman, 2008). Because K$^+$ transport is rate-limiting, counterion (Cl$^-$) movement was taken implicitly to accompany K$^+$ uptake into astrocytes to maintain electroneutrality. Water transport across the astrocyte–ECS interface is driven osmotically from the difference in ECS and astrocyte osmolalities (sum of K$^+$ and non-K$^+$ solutes). AQP4 deletion was modeled as reduced astrocyte water permeability. Water transport between the ECS and astrocyte compartments results in displacement of the astrocyte–ECS interface, with water uptake causing ECS contraction and astrocyte expansion. In the well-mixed model, the ECS and astrocyte compartments were taken as well-stirred. In the diffusion-limited model, solute (K$^+$ and non-K$^+$) movement in astrocyte cytoplasm is diffusion-limited. The characteristics of the well-mixed and diffusion-limited models are first presented, investigating a broad range of model parameters. We then focus on the model parameters needed to account for experimental observations on effects of AQP4 deletion on K$^+$ accumulation and reuptake from the ECS during and after neuroexcitation. Fig. 2

diagrams the computational approach, as detailed in the Model computations section.

Well-mixed model

In the well-mixed model, K$^+$ and non-K$^+$ solutes distribute instantaneously in the ECS and astrocyte compartments in response to K$^+$ and water transport (Fig. 3 A). Water uptake by astrocytes causes ECS shrinkage. Based on experimental data (Ransom et al., 1985), initial (resting) K$^+$ concentrations, compartment volumes, and membrane potential were taken as: $[K^+]_e = 5$ mM, $[K^+]_a = 140$ mM, $d_e = 2$ µm, $d_a = 10$ µm, and $\psi = -83$ mV. A starting parameter set ($P_K = 1.2 \times 10^{-5}$ cm/s, $J_{K^o}^n = 10^{-8}$ mol/cm^2/s, $J_{K\,pump}^a(0) = -2.2 \times 10^{-11}$ mol/cm^2/s) was specified to: (a) maintain stable $[K^+]_e$ before neuroexcitation; (b) increase $[K^+]_e$ from 5 to 10 mM during brief neuroexcitation; and (c) return $[K^+]_e$ to 5 mM with $t_{1/2} \sim 5$ s (Fig. 3 B).

Fig. 3 B shows the behavior of the well-mixed model for a water permeable astrocyte membrane ($P_f = 0.04$ cm/s). After brief (0.1 s) release of K$^+$ by neurons into the ECS
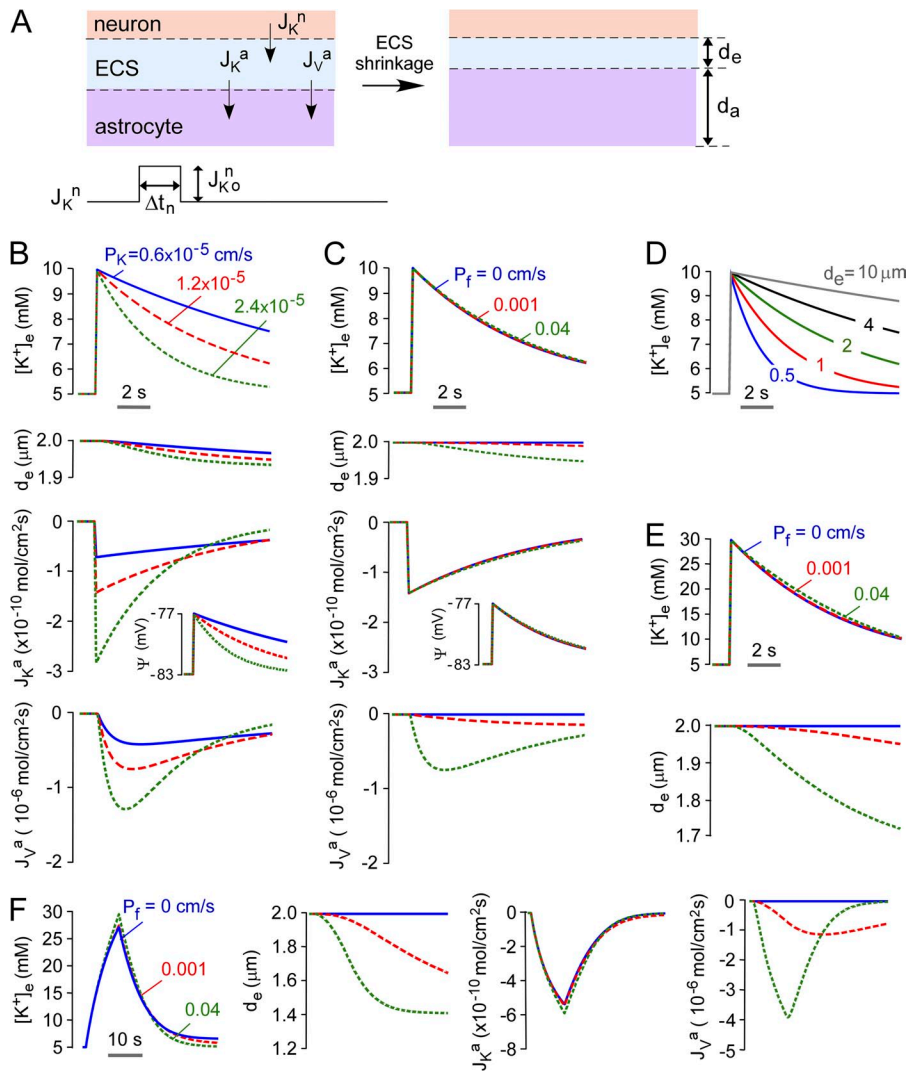

Figure 3. Predictions of the well-mixed model. (A) Schematic of well-mixed model showing neuronal K$^+$ release into ECS, and astrocytic uptake of K$^+$ and water causing ECS shrinkage. (B) Time course of ECS potassium concentration ($[K^+]_e$) and volume (d_e), astrocyte membrane potential (ψ), and astrocyte K$^+$ and water flux (J_K^a, J_V^a) after neuronal excitation causing $[K^+]_e$ increase from 5 to 10 mM. Parameters: $P_f = 0.04$ cm/s, $J_{K^o}^n = 10^{-8}$ mol/cm^2/s, $\Delta t_n = 0.1$ s, $d_a = 10$ µm, $d_e = 2$ µm, with the indicated P_K. (C) Computations as in B for $P_K = 1.2 \times 10^{-5}$ cm/s with the indicated P_f. (D) Computations as in B for $P_K = 1.2 \times 10^{-5}$ cm/s, with the indicated d_e. $J_{K^o}^n$ was adjusted to increase $[K^+]_e$ from 5 to 10 mM. (E) Effect of magnitude of neuroexcitation. Computations as in B, with $P_K = 1.5 \times 10^{-5}$ cm/s and $J_{K^o}^n = 5 \times 10^{-8}$ mol/cm^2/s, with the indicated P_f. (F) The effect of duration of neuroexcitation. Computations as in B, with $P_K = 1.3 \times 10^{-5}$ cm/s, $J_{K^o}^n = 8 \times 10^{-10}$ mol/cm^2/s, and $\Delta t_n = 10$ s, with the indicated P_f.

to increase $[K^+]_e$ from 5 to 10 mM, $[K^+]_e$ returned to baseline at a rate determined by P_K. ECS contraction was minimal, <3%. J_K^a and ψ changed rapidly after the increase in $[K^+]_e$ and returned over time to baseline. Changes in J_v^a lagged because the finite water permeability prevents instantaneous osmotic equilibration. Fig. 3 C shows little effect of P_f on the kinetics of $[K^+]_e$. Though reduced P_f altered the kinetics of J_K^a and J_v^a, as predicted, the relatively small magnitude of K^+ uptake (5 mM) compared with total ECS/astrocyte solute content translated to minimal effect on $[K^+]_e$. Fig. 3 D shows the influence of ECS volume, d_e, on the kinetics of $[K^+]_e$, in which neuronal K^+ release was adjusted to maintain the increase in $[K^+]_e$ from 5 to 10 mM. At constant P_K, increasing d_e slowed the kinetics of K^+ reuptake because of the greater quantity of K^+ taken up by astrocytes to return $[K^+]_e$ to baseline.

The minor effect of P_f in the well-mixed model is related, in part, to the small amount of K^+ taken up by astrocytes compared with the total solute content. To investigate whether P_f could influence the kinetics of $[K^+]_e$ when ECS shrinkage was more substantial, computations were done with greater and more prolonged neuronal K^+ release. Fig. 3 E shows that increasing neuronal K^+ release to give peak $[K^+]_e$ of 30 mM, though producing greater ECS shrinkage, conferred little sensitivity of $[K^+]_e$ to P_f. Fig. 3 F shows that increasing the duration of neuronal K^+ release from 0.1 to 10 s further increased ECS shrinkage, but again conferred little sensitivity of $[K^+]_e$ to P_f. Prolonged neuronal K^+ release greatly increased the total amount of K^+ taken up by astrocytes because uptake occurs concurrently with neuronal K^+ release. This produced a mild slowing of the return of $[K^+]_e$ to baseline because K^+ added to the ECS is diluted into a greater volume with consequent reduced driving force. Further computations using the well-mixed model are done below (see Fig. 6) for modeling of experimental data.
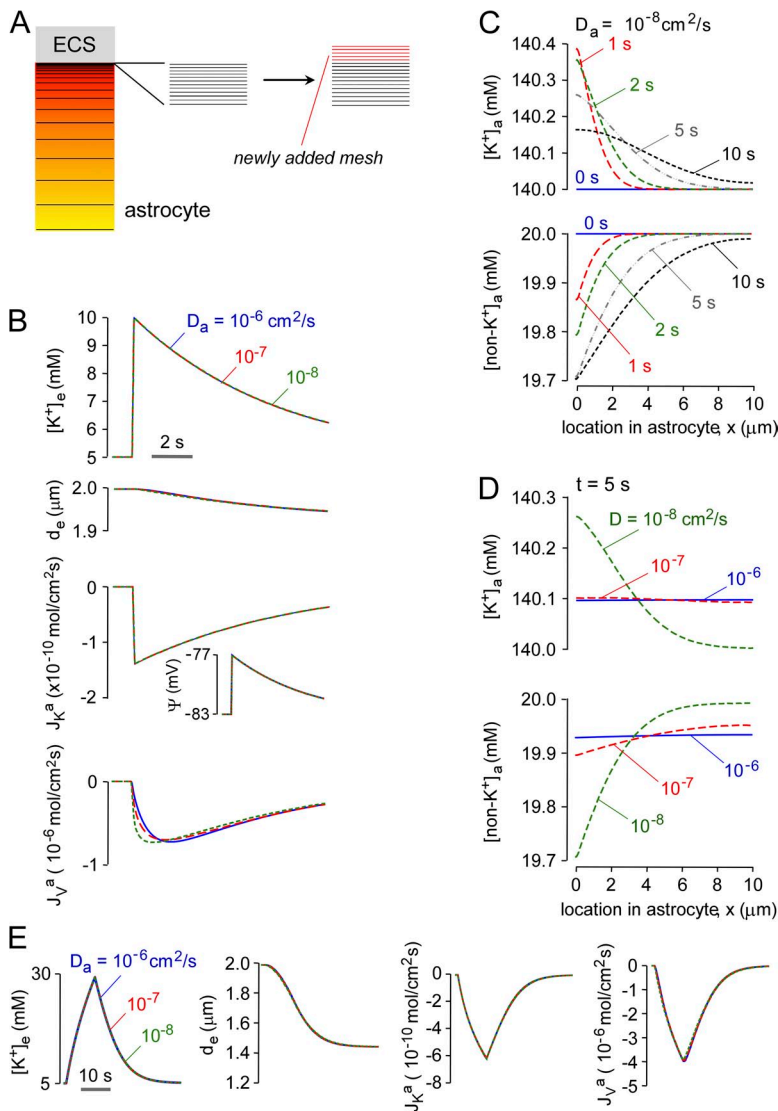
Figure 4. Predictions of the diffusion-limited model for high astrocyte water permeability. $P_f = 0.04$ cm/s for computations in this figure. (A) Schematic showing nonlinear and newly added mesh elements in astrocyte cytoplasm used for numerical solution of the diffusion equation. See text for explanation. (B) Time course of $[K^+]_e$, d_e, ψ, J_K^a, and J_v^a after neuroexcitation for the indicated cytoplasmic diffusion coefficients, D_a. Parameters: $P_K = 1.2 \times 10^{-5}$ cm/s, $J_K^{n}{}_o = 10^{-8}$ mol/cm^2/s, $\Delta t_n = 0.1$ s, $d_a = 10$ µm, and $d_e = 2$ µm. (C and D) Astrocyte spatial distribution of $[K^+]_a$ and $[non-K^+]_a$ at the indicated times, with parameters as in B, for $D_a = 10^{-8}$ cm^2/s (C) and t = 5 s (D). (E) Effect of duration of neuroexcitation. Computations as in B, with $P_K = 1.3 \times 10^{-5}$ cm/s, $J_K^{n}{}_o = 8 \times 10^{-10}$ mol/cm^2/s, and $\Delta t_n = 10$ s.

Diffusion-limited model

We reasoned that restricting solute diffusion could amplify the influence of P_f on the kinetics of $[K^+]_e$ by a pseudo-solvent drag-like mechanism. In the diffusion-limited model, diffusion of K^+ and non-K^+ solutes in astrocyte cytoplasm was described by a diffusion coefficient, D_a. Diffusion of K^+ and non-K^+ solutes occurs after transport of K^+ and water from the ECS into the astrocyte cytoplasm. Buildup of K^+ near the astrocyte–ECS interface (and dilution of non-K^+ solutes) with finite D_a alters the electrochemical driving force for K^+ transport and the osmotic driving force for water transport, conferring model sensitivity to D_a. As detailed in the supplemental text, a novel mathematical approach was developed to compute K^+ and water transport/diffusion for a nonstationary astrocyte–ECS interface resulting from water influx. Our approach involved the addition of newly created mesh elements to a nonuniform mesh after K^+ and water influx across the astrocyte–ECS interface (Fig. 4 A), "buffering" to eliminate effects of near-interfacial discontinuities, and computation of the diffusion of K^+ and non-K^+ solutes in the cytoplasmic compartment. The electrochemical driving force for K^+ transport and the osmotic driving force for water transport were computed from concentrations of K^+ and non-K^+ solutes in astrocyte cytoplasm at the ECS-facing limiting membrane.

The predictions of the diffusion-limited model were first examined for a water-permeable astrocyte membrane ($P_f = 0.04$ cm/s) and for brief (0.1 s) neuroexcitation. Fig. 4 B shows little effect of D_a on $[K^+]_e$, d_e, J_K^a, and J_v^a for a 100-fold range in D_a from 10^{-6} to 10^{-8} cm^2/s. Fig. 4 C shows the time evolution of the cytoplasmic spatial profiles of $[K^+]_a$ and $[\text{non-}K^+]_a$ for D_a of 10^{-8} cm^2/s. Because of the diffusion-limited redistribution of K^+ in astrocyte cytoplasm, $[K^+]_a$ was relatively concentrated at early times (albeit to a small extent when P_f is high) near the astrocyte–ECS interfacial membrane and reduced far from the interface. The spatial inhomogeneity in $[K^+]_a$ dissipated over time. The spatial profile of $[\text{non-}K^+]_a$ showed relative dilution near the astrocyte–ECS interface. Fig. 4 D shows the spatial profiles of $[K^+]_a$ and $[\text{non-}K^+]_a$ at 5 s at different D_a. Greater inhomogeneity, albeit quite small, was seen with reduced D_a, as expected. To investigate whether greater ECS shrinkage confers a greater influence of D_a on the kinetics of $[K^+]_e$ and on the inhomogeneity of $[K^+]_a$, computations were done with greater neuronal K^+ release and duration, as was done for the well-mixed model in Fig. 3 F. Fig. 4 E shows little effect of D_a on $[K^+]_e$, d_e, J_K^a, and J_v^a with high P_f, even under conditions of greater ECS shrinkage. High P_f prevented substantial buildup of K^+ near the astrocyte–ECS interface.

Fig. 5 A shows the effect of reduced P_f on the kinetics of $[K^+]_e$ for brief (0.1 s) neuroexcitation. With astrocyte K^+ release adjusted to increase $[K^+]_e$ from 5 to 10 mM, reduced D_a had little effect on the kinetics of $[K^+]_e$ return. Slight slowing was seen at reduced P_f when $[K^+]_e$ was increased to 30 mM (Fig. 5 B), producing greater ECS shrinkage. Increasing $[K^+]_e$ with prolonged neuronal K^+ release (Fig. 5 C) produced greater ECS K^+ accumulation and faster recovery at high P_f because of greater ECS shrinkage. As shown in Fig. 5 D, the slowed return of $[K^+]_e$ in the diffusion-limited model for low D_a is the consequence of buildup of K^+ at the astrocyte–ECS interface, which is amplified at low P_f because of the impaired astrocyte swelling response.

Modeling experimental data on ECS K^+ dynamics in AQP4 deficiency

Having characterized model predictions, three sets of experimental observations on brain/brain slices from AQP4 knockout mice were modeled to test the hypothesis that AQP4-dependent K^+ dynamics in the ECS are explicable on the basis of physicochemical considerations alone, without requiring altered astrocyte K^+ conductance in AQP4 deficiency. Modeling was done for wild-type versus AQP4-deficient astrocytes, testing effects of ECS expansion in AQP4 deficiency ($d_e = 2$ vs. 2.4 µm) and restricted astrocyte diffusion.

The first set of experimental observations involves a hippocampal brain slice model in which brief electrical stimulation (0.1 ms) produced small increases in $[K^+]_e$, which were reduced in magnitude in brain slices from AQP4 knockout mice (Strohschein et al., 2011). Fig. 6 A shows computations in the well-mixed and diffusion-limited models with identical neuroexcitation strength and duration. Both models predicted an ~20% reduction in maximum $[K^+]_e$ in AQP4 deficiency only when ECS expansion ($d_e = 2.4$) was considered, which is in agreement with experimental data showing an ~20% reduced increase in $[K^+]_e$ in brain slices from AQP4 knockout mice. AQP4 deficiency did not affect the $t_{1/2}$ for return of $[K^+]_e$ to baseline, which agreed with model predictions.

The second set of experimental observations involves a larger increase in $[K^+]_e$. In the hippocampal brain slice model, repetitive stimuli (20 Hz for 10 s) produced smaller increases and slowed recovery of $[K^+]_e$ in the stratum pyramidale of AQP4 knockout mice (Strohschein et al., 2011). In an in vivo direct cortical stimulation model, AQP4 deficiency produced a delay in the rise and recovery of $[K^+]_e$ after 1 s of stimulation (Binder et al., 2006). The repetitive pulsed simulation protocol was modeled, which predicted a smaller reduction in the increase in $[K^+]_e$ when ECS expansion in AQP4 deficiency was considered (Fig. 6 B, left and center), as found experimentally. The model also predicted the experimentally observed slowed recovery, as quantified by higher $[K^+]_e$ at 20 s after stimulation in AQP4-deficient versus wild-type brain slices (Fig. 6 B, right, top) and slower relative $t_{1/2}$ (Fig. 6 B, right, bottom). ECS expansion

(d_e = 2.4) in AQP4 deficiency slightly slowed the recovery (Fig. 6 B, left and center). The slowed return of $[K^+]_e$ to baseline in AQP4 deficiency increases neuronal sensitivity in a nonlinear manner, causing prolonged neuronal firing and seizure activity, as found experimentally (Binder et al., 2006). To quantify the fold change in P_f required for substantial alteration of ECS K^+ dynamics in our model, the relative change in $t_{1/2}$ (on a normalized y scale) is plotted as a function of P_f (Fig. 6 B, inset), showing 50% change in $t_{1/2}$ for less than a 10-fold change in P_f.

The third set of experimental observations involves a model of cortical spreading depression, which is produced by propagating K^+ waves in brain, resulting in a sustained increase in $[K^+]_e$ to > 25 mM. In a mechanical stimulation (pin-prick) model of spreading depression, AQP4 knockout mice showed approximately twofold slowed recovery in $[K^+]_e$ (Padmawar et al., 2005). Fig. 6 C shows predicted $[K^+]_e$ for a 30-s stimulation producing an increase in $[K^+]_e$ from 5 to 25 mM. AQP4 deficiency without ECS expansion (d_e = 2 μM) slowed $[K^+]_e$ recovery by ~20%, with ~50% slowing when ECS expansion was included (d_e = 2.4). A slowing of $[K^+]_e$ recovery of approximately twofold, as found experimentally, was predicted in the diffusion-limited model when restricted

$[K^+]_e$ diffusion was included. Fig. 6 C (inset) shows that a 50% change in $t_{1/2}$ occurred for a ~10-fold change in P_f.

Last, as described in the supplemental text, the robustness of key model assumptions about astrocyte K^+ influx mechanisms and geometry was considered. Computations were done: (a) for an expanded astrocyte with d_e of 100 μm, (b) with inclusion of electroneutral (membrane potential–independent) K^+ influx mechanisms representing astrocytic NKCC and KCC-facilitated K^+ uptake, and (c) with nonuniform ECS thickness. Notwithstanding uncertainties in the selection of parameters required to model more complex transport mechanisms and ECS geometry, we found that the major model predictions with regard to P_f and diffusion-limited effects were insensitive to the precise ECS, the magnitude of electroneutral K^+ influx, or the K^+-coupling factor used in computations.

DISCUSSION

The modeling here provided new insights on the mechanisms of apparent coupling of K^+ and water transport in brain ECS and on the role of astrocyte water permeability in K^+ homeostasis in neuroexcitation. K^+ uptake
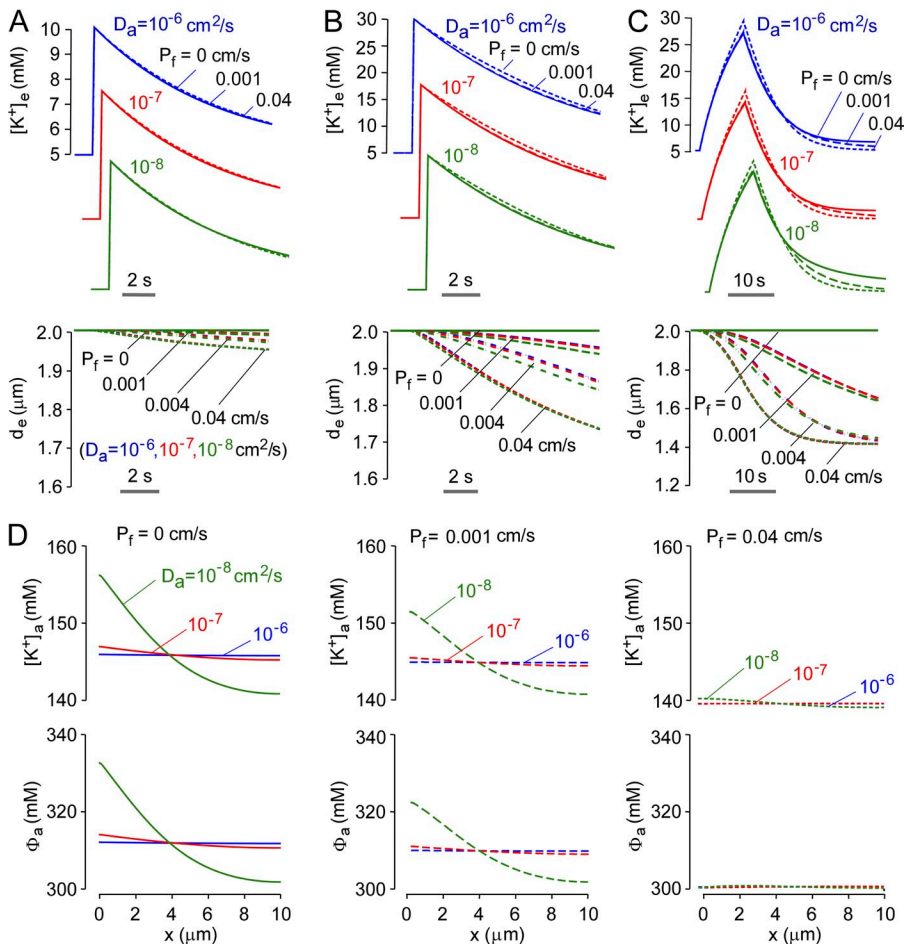
Figure 5. Water permeability effects in the diffusion-limited model. (A) Time course of $[K^+]_e$ and d_e for the indicated P_f and D_a. Parameters: P_K = 1.2×10^{-5} cm/s, $J_{K^n_o}$ = 10^{-8} mol/cm^2/s, Δt_n = 0.1 s, d_a = 10 μm, and d_e = 2 μm. (B) Effect of magnitude of neuroexcitation. Computations as in B, but with $J_{K^n_o}$ = 5×10^{-8} mol/cm^2/s to increase $[K^+]_e$ from 5 to 30 mM. (C) Effect of duration of neuroexcitation. Computations as in C, with P_K = 1.3×10^{-5} cm/s, $J_{K^n_o}$ = 8×10^{-10} mol/cm^2/s, and Δt_n = 10 s. (D) Spatial distributions of $[K^+]_a$ and osmolarity (Φ_a) in astrocyte cytoplasm for the indicated P_f and D_a, with parameters as in C.

by astrocytes in response to release from neurons produces an osmotic driving force for water uptake by astrocytes, which reduces ECS volume and hence contributes to maintaining the electrochemical driving force for continued K^+ uptake. Reduced astrocyte water permeability in AQP4 deficiency slows the change in ECS volume, resulting in slowed decay of $[K^+]_e$. Inclusion of diffusion-limited solute transport in the model amplified the sensitivity of K^+ uptake to P_f by a pseudo-solvent drag-like mechanism in which buildup of K^+ in astrocyte cytoplasm at the ECS interface reduced the driving force for K^+ uptake in a P_f-dependent manner. The modeling made predictions about the magnitude of reduction in astrocyte water permeability needed to account for experimental data, as well as solute diffusion in astrocyte cytoplasm.

Our results support the possibility that loss of AQP4-dependent water transport can account for neuroexcitation phenotypes in AQP4 deficiency, without requiring direct AQP4/K^+ channel coupling or alterations in astrocyte properties in AQP4 deficiency. The experimentally observed mild ECS expansion in AQP4 deficiency was necessary and sufficient to account for the reduced accumulation of K^+ in the ECS during single or pulsed neuroexcitation. The slowed kinetics of K^+ reuptake from the ECS after neuroexcitation was explained largely by indirect coupling of K^+ and water transport involving dynamic ECS contraction in the well-mixed model, in which reduced astrocyte water permeability slowed ECS contraction and thus altered the electrochemical driving force for astrocyte K^+ reuptake. However, quantitative agreement between model predictions and experimental observations on K^+ reuptake required diffusion-limited solute transport in astrocyte cytoplasm, which amplified the effects of reduced P_f by creating a nonuniform spatial profile of K^+ in astrocyte cytoplasm with buildup of K^+ near the plasma membrane. The K^+ near the plasma membrane is diluted by water flux from the ECS into the astrocyte, opposing K^+ buildup and maintaining membrane potential.

Our model focused on the question of under what conditions can electrochemical/osmotic coupling of
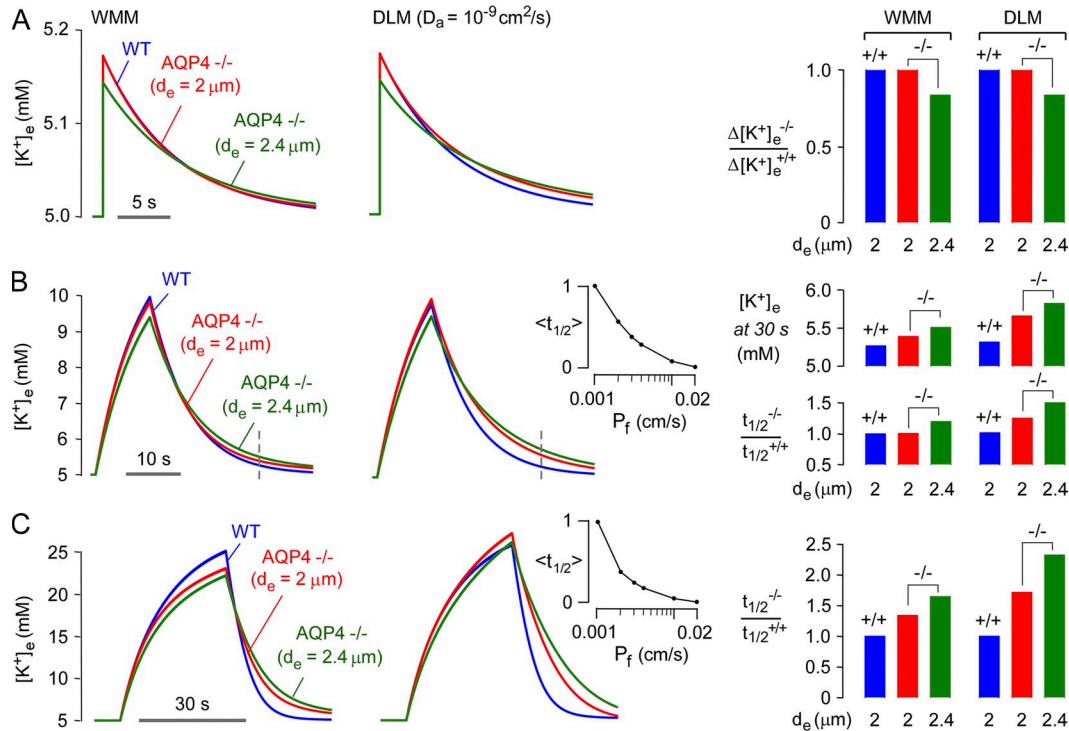
Figure 6. Modeling of experimental observations of altered K^+ dynamics in AQP4 deficiency. (A) Single neuron firing ($\Delta t_n = 0.1$ ms). Time course of $[K^+]_e$ modeled for wild type (WT) mice ($P_f = 0.04$ cm/s) and AQP4 knockout mice (AQP4$^{-/-}$, $P_f = 0.001$ cm/s, $d_e = 2$ or 2.4 µm) for well-mixed model (WMM, left) and diffusion-limited model (DLM, $D_a = 10^{-9}$ cm^2/s, center). Parameters: $P_K^a = 1.2 \times 10^{-5}$ cm/s, $J_{K^o}^n = 3.5 \times 10^{-7}$ mol/cm^2/s, and $\Delta t_n = 0.1$ ms. (right) Relative increase $[K^+]_e$ after neuroexcitation in WT vs. AQP4 knockout mice ($\Delta[K^+]_e^{-/-}/\Delta[K^+]_e^{+/+}$). (B) Repetitive pulsed neuronal excitation. (left and center) $[K^+]_e$ in response to 20 Hz stimulation ($\Delta t_n = 0.1$ ms firing) for 10 s. Parameters: $P_K^a = 1.2 \times 10^{-5}$ cm/s and $J_{K^o}^n = 2.1 \times 10^{-7}$ mol/cm^2/s. (right) $[K^+]_e$ at 20 s (broken line) after neuroexcitation and relative half-times for return of $[K^+]_e$ to baseline ($t_{1/2}^{-/-}/t_{1/2}^{+/+}$). (inset) P_f dependence of $t_{1/2}$ in the DLM (at fixed d_e of 2 µm), shown on a normalized y scale (denoted $\langle t_{1/2}\rangle$). A similar P_f dependence was seen for $[K^+]_e$ (not depicted). (C) Prolonged neuronal firing. (left and center) $[K^+]_e$ responses to 20 Hz stimulation for 30 s. Parameters: $P_K^a = 1.2 \times 10^{-5}$ cm/s and $J_{K^o}^n = 3.45 \times 10^{-7}$ mol/cm^2/s. (right) Summary of $t_{1/2}^{-/-}/t_{1/2}^{+/+}$. (inset) P_f dependence of $\langle t_{1/2}\rangle$ in the DLM (at fixed d_e of 2 µm), shown on a normalized y scale.

K$^+$ and water transport account for the effects of AQP4 deletion on K$^+$ and water dynamics after neuroexcitation. Our model did not attempt to describe the complex three-dimensional geometry of brain cells and ECS, or the details of astrocyte K$^+$ uptake mechanisms involving K$^+$ channels, NKCC and KCC K$^+$ cotransporters, and the Na$^+$/K$^+$ pump. We did not model long-range K$^+$ spatial buffering and hence did not include the complexities of ion field migration in cytoplasm. To focus on K$^+$/water transport coupling, we felt it was important to minimize the complexity of the model and the number of variables and parameters; the main parameters were K$^+$ and volume, without explicit modeling of Na$^+$ and Cl$^-$, which would add so many variables as to negate the predictive value of the model. Electroneutrality was applied implicitly, considering both conductive and electroneutral K$^+$ entry mechanisms. With constraints imposed by experimental data, our model was highly constrained, allowing focused investigation of parameter space, including P_f, d_e, J_K^n, Δt_n, and D_a. Electroneutral transport (NKCC and KCC), which was modeled separately, had little influence on key model predictions. Though model computations used one-dimensional geometry with uniform ECS thickness, the potential influences of more complex geometry were in effect considered by variations in d_e and d_a, and in D_a. Also, computations done for a nonuniform ECS thickness did not affect key model predictions. Further refinement of the model here is anticipated as more experimental data become available on the kinetics of ECS K$^+$ and volume following different types of neuroexcitation, as well as on ECS geometry and astrocyte transport mechanisms.

The modeling showed that a reduction in P_f, to simulate AQP4 knockout, predicted many of the observed qualitative features of the experimental data. The analysis in Fig. 6 showed that 50% of maximal effect on K$^+$ dynamics (produced by increasing P_f from 0 to a very high level) required an ∼10-fold change in P_f. A sevenfold reduction in P_f was measured in well-differentiated astrocyte cultures from cortex of neonatal AQP4-deficient mice (Solenov et al., 2004). However, it is not possible to extrapolate absolute or relative P_f (in AQP4 deficiency) from cell cultures to brain in vivo because of differences in AQP4 polarization, cell geometry (surface-to-volume ratio), and AQP4 expression. It is likely that the fold reduction in P_f in AQP4 deficiency is 10 or greater in vivo based on the remarkable brain protection in models of cytotoxic edema, including water intoxication (Manley et al., 2000), and the much slowed brain water uptake after water intoxication as measured by infrared scattering (Thiagarajah et al., 2005). In cells outside of the brain, AQPs generally increase water permeability by 10-fold or greater (Verkman, 2012).

In prior modeling of ECS dynamics, Østby et al. (2009) did similar computations to the well-mixed model here,

though their model explicitly included K$^+$, Cl$^-$, Na$^+$, and HCO$_3^-$, and their associated transporters, NKCC1, KCC1, and NBC. In addition to not considering diffusion-limited solute transport, other major differences in the Østby et al. (2009) model include allowance of water transport through NKCC1, which was necessary to account for the experimental data, and lack of inclusion the Kir4.1 K$^+$ channel. As such, their interpretation of mechanisms of ECS volume and K$^+$ dynamics are quite different from those here. Østby et al. (2009) concluded that none of the major basic membrane processes (Na/K/ATPase pump, passive ion transport, and osmotically driven water transport), or the added contribution from KCC1, were able to predict experimentally observed ECS shrinkage, though the combined action of NBC and NKCC1, together with NKCC1-dependent water transport, increased ECS shrinkage to experimentally observed levels. We would question the conclusions regarding NKCC1 of Østby et al. (2009), as NKCC1 deletion had a minimal effect on K$^+$ reuptake after application of high extracellular K$^+$ (Su et al., 2002). Our model here accounts for experimental observations, without reliance on major electroneutral K$^+$ transport or non-AQP4 water transport pathways, providing a simple explanation of observed ECS K$^+$/water dynamics.

Several experimental studies have been reported on astrocyte K$^+$ transporting mechanisms, though some with conflicting results. Kir4.1 is the major K$^+$ buffering channel in astrocytes, with >80% reduction in K$^+$ conductance after neuroexcitation with Ba^{2+} inhibition (Meeks and Mennerick, 2007); Kir4.1 knockout depolarizes astrocyte membrane potential, from −80 mV to −45 to −60 mV (Djukic et al., 2007; Chever et al., 2010). The quantitative role of Kir4.1 in ECS K$^+$ clearance, however, has been controversial, in part because of the different experimental systems and measurement methods. Two recent studies in Kir4.1 knockout mice showed slowed recovery of [K$^+$]$_o$ after neuroexcitation. Haj-Yasein et al. (2011a) showed approximately twofold slowed recovery after 10 s of high-frequency (20 Hz) stimulation; Chever et al. (2010) showed approximately twofold slowed recovery of [K$^+$]$_o$ after 0.5–2 s of high-frequency (10 Hz) stimulation, but failed to see any difference after 30 s of stimulation. Jauch et al. (2002) showed a greater increase in ECS K$^+$ after Ba^{2+} in response to a glutamate receptor agonist. However, other studies did not show significant effects of Ba^{2+} in brain slices, optic nerve, and retina (Xu and Karwoski, 1994; Ransom et al., 2000; D'Ambrosio et al., 2002; Meeks and Mennerick, 2007).

NKCC1 may be also involved in K$^+$ buffering. Several older studies showed partial reduction in stimulus and K$^+$-evoked ECS shrinkage by the NKCC1 inhibitors bumetanide and furosemide, using intrinsic optical signal and tetramethylammonium measurement methods (Ransom et al., 1985; MacVicar et al., 2002). Studies in

astrocyte cell cultures suggest a greater contribution from NKCC1 versus Kir4.1 for high ECS K$^+$ (>20 mM) than for low ECS K$^+$ (<10 mM). Furosemide inhibited K$^+$ influx by up to 50% at high ECS K$^+$ (Walz and Hertz, 1982; Walz and Hinks, 1985). NKCC1 knockout reduced K$^+$ influx by ~20% at high ECS K$^+$ (Su et al., 2002). Notwithstanding the different methods and systems studied, the available evidence supports the involvement of both conductive and electroneutral astrocytic K$^+$ transporting mechanisms, whose exact contributions are not clear and may change under different experimental conditions. The bulk of modeling in the paper assumed conductive astrocyte K$^+$ uptake, though computations shown in the supplemental text, which include both conductive and electroneutral K$^+$ uptake, show that the major conclusions regarding effects of astrocyte water permeability and solute diffusion are robust and insensitive to the precise relative contribution of electroneutral K$^+$ uptake.

In general, modeling of membrane transport requires the selection of modeling equations and parameters, which, for the modeling of ECS K$^+$/water dynamics here, is made challenging because of inconsistencies in the literature about the role of Kir4.1 and conductive versus neutral K$^+$ transport in astrocyte swelling and K$^+$ uptake, as mentioned in the previous paragraph, as well as the quite different experimental conditions such as the size, duration, and type of stimulus used to increased ECS K$^+$, and the various in vitro (astrocyte culture, brain slice, optic nerve) and in vivo model systems used. Model parameters for our computations came largely from experimental data in brain slices and optic nerve, though our conclusions are robust and did not depend on exact model parameters. Resting [K$^+$]$_e$ from K$^+$-selective electrode measurements in intact brain and ex vivo brain slices, as well as optic nerve, range from 3 to 5 mM. We chose [K$^+$]$_e$ = 5 mM from data in hippocampal slices and optic nerve (Ransom et al., 1985; Sick et al., 1987). ECS volume was taken as d_e = 2 μm, based on an mean astrocyte diameter of 10 μm (Allen and Barres, 2009) and an ECS volume fraction of 0.20 from tetramethylammonium (Syková and Nicholson, 2008) and fluorescent dye partitioning (Zhang and Verkman, 2010) measurements. Membrane potential was chosen as −83 mV based on the experimental relationship of [K$^+$]$_e$ and membrane potential in astrocytes (Chow et al., 1991). In brain slice studies, there is a "ceiling" level of 10–12 mM [K$^+$]$_e$ in response to prolonged maximal stimulation (Somjen, 1979), which was not modeled here because of uncertainties in its mechanism and relevance to the in vivo brain. In some computations, [K$^+$] was increased from 5 to 30 mM to simulate cortical spreading depression.

Additional caveats should be noted in comparing model predictions to experimental data. Because AQP4 inhibitors are not available, data were taken from studies in AQP4 knockout mice. In general, studies done in knockout mice are potentially confounded by altered expression of many genes, and, consequently, there may be phenotype changes that do not result directly from deletion of the gene of interest. In the case of AQP4 knockout mice, mild ECS volume expansion at baseline (Binder et al., 2004; Yao et al., 2008; Zhang and Verkman, 2010), mildly increased brain water content (Haj-Yasein et al., 2011b), greater shrinkage of the ECS in the hippocampal CA1 region during neuroactivation (Haj-Yasein et al., 2012), reduced perivascular expression of α-syntrophin and dystrophin (Eilert-Olsen et al., 2012), reduced expression of a glutamate transporter (GLT-1; Zeng et al., 2007), and possibly altered cx43 expression (Strohschein et al., 2011) have all been reported. Impaired tissue water clearance has been consistently reported in AQP4 knockout mice, so prolonged astrocyte swelling after hippocampal stimulation could account for increased ECS shrinkage in the CA1 stratum radiatum (compartment with glial perisynaptic astrocyte processes; Haj-Yasein et al., 2012). Our model predicts that astrocyte swelling, and hence ECS shrinkage, accompanies astrocytic water and K$^+$ influx. Similarly, slowed efflux of intracellular astrocytic water after neuroexcitation could account for prolonged ECS shrinkage in AQP4 deficiency, a parsimonious explanation for the Haj-Yasein et al. (2012) results and consistent with our previous data (Binder et al., 2006). Though the effect of AQP4 deletion on ECS volume was taken into account in the modeling, it is difficult to evaluate the potential effects of other reported changes in AQP4 deficiency. More pertinent experimental studies await AQP4-selective inhibitors, if and when they will become available.

A technical challenge in the diffusion-limited model was the computation of coupled transport and diffusion of K$^+$ and water for a nonstationary membrane interface. Our approach involved transport of K$^+$ and water into a buffer zone in astrocyte cytoplasm adjacent to the membrane interface, and computation of diffusion of K$^+$ and non-K$^+$ solutes in cytoplasm. We assumed diffusion-limited redistribution only in astrocyte cytoplasm because diffusion in cytoplasm is expected to be slower than in the ECS (Dix and Verkman, 2008), and because cytoplasmic volume is much greater than ECS volume. The moving boundary problem was solved using a nonuniform mesh with new mesh elements added near the plasma membrane with astrocyte expansion. The mesh elements were populated by newly transported K$^+$ and water in a buffer zone, with subsequent redistribution of K$^+$ and non-K$^+$ solutes by diffusion. To our knowledge, this strategy has not been used previously for computations of diffusion with a moving boundary. The modeling approach here can be extended to investigate additional details of K$^+$/water coupling. For example, AQP4 and Kir4.1 are highly expressed on astrocyte end-feet in contact with the blood vessels. Impaired polarization of

AQP4 expression, which was associated with prolonged thermally induced seizures (Amiry-Moghaddam et al., 2003), has been reported in α-syntrophin knockout mice. Modeling may be informative to investigate the importance of perivascular transporter polarization for efficient ECS K^{+} clearance.

In conclusion, notwithstanding the caveats discussed above, our model supports the conclusion that ECS contraction during K^{+} uptake by astrocytes after neuro-excitation, together with mild ECS expansion in AQP4 deficiency, can account for experimental observations on AQP4-dependent ECS K^{+}/water dynamics. Thus, K^{+}/water coupling in the ECS is potentially explicable on the basis of physicochemical principles alone, without requiring assumptions about altered astrocyte K^{+} permeability in AQP4 deficiency or NKCC-mediated water permeability. Our modeling thus accounts for the P_f sensitivity of K^{+} accumulation into and uptake from the ECS with neuroexcitation, and provides a potential explanation for observed effects of AQP4 deficiency on seizure dynamics, cortical spreading depression, and neurosensory signaling.

REFERENCES

Allen, N.J., and B.A. Barres. 2009. Neuroscience: Glia - more than just brain glue. *Nature.* 457:675–677. http://dx.doi.org/10.1038/457675a

Amiry-Moghaddam, M., A. Williamson, M. Palomba, T. Eid, N.C. de Lanerolle, E.A. Nagelhus, M.E. Adams, S.C. Froehner, P. Agre, and O.P. Ottersen. 2003. Delayed K^{+} clearance associated with aquaporin-4 mislocalization: phenotypic defects in brains of alpha-syntrophin-null mice. *Proc. Natl. Acad. Sci. USA.* 100:13615–13620. http://dx.doi.org/10.1073/pnas.2336064100

Auguste, K.I., S. Jin, K. Uchida, D. Yan, G.T. Manley, M.C. Papadopoulos, and A.S. Verkman. 2007. Greatly impaired migration of implanted aquaporin-4-deficient astroglial cells in mouse brain toward a site of injury. *FASEB J.* 21:108–116. http://dx.doi.org/10.1096/fj.06-6848com

Ballanyi, K., P. Grafe, and G. ten Bruggencate. 1987. Ion activities and potassium uptake mechanisms of glial cells in guinea-pig olfactory cortex slices. *J. Physiol.* 382:159–174.

Bay, V., and A.M. Butt. 2012. Relationship between glial potassium regulation and axon excitability: a role for glial Kir4.1 channels. *Glia.* 60:651–660. http://dx.doi.org/10.1002/glia.22299

Binder, D.K., M.C. Papadopoulos, P.M. Haggie, and A.S. Verkman. 2004. In vivo measurement of brain extracellular space diffusion by cortical surface photobleaching. *J. Neurosci.* 24:8049–8056. http://dx.doi.org/10.1523/JNEUROSCI.2294-04.2004

Binder, D.K., X. Yao, Z. Zador, T.J. Sick, A.S. Verkman, and G.T. Manley. 2006. Increased seizure duration and slowed potassium kinetics in mice lacking aquaporin-4 water channels. *Glia.* 53:631–636. http://dx.doi.org/10.1002/glia.20318

Chen, K.C., and C. Nicholson. 2000. Spatial buffering of potassium ions in brain extracellular space. *Biophys. J.* 78:2776–2797. http://dx.doi.org/10.1016/S0006-3495(00)76822-6

Chever, O., B. Djukic, K.D. McCarthy, and F. Amzica. 2010. Implication of Kir4.1 channel in excess potassium clearance: an in vivo study on anesthetized glial-conditional Kir4.1 knock-out mice. *J. Neurosci.* 30:15769–15777. http://dx.doi.org/10.1523/JNEUROSCI.2078-10.2010

Chow, S.Y., Y.C. Yen-Chow, H.S. White, L. Hertz, and D.M. Woodbury. 1991. Effects of potassium on the anion and cation contents of primary cultures of mouse astrocytes and neurons. *Neurochem. Res.* 16:1275–1283. http://dx.doi.org/10.1007/BF00966658

D'Ambrosio, R., D.S. Gordon, and H.R. Winn. 2002. Differential role of KIR channel and Na^{+}/K^{+}-pump in the regulation of extracellular K^{+} in rat hippocampus. *J. Neurophysiol.* 87:87–102.

Dietzel, I., U. Heinemann, G. Hofmeier, and H.D. Lux. 1982. Stimulus-induced changes in extracellular Na^{+} and Cl^{-} concentration in relation to changes in the size of the extracellular space. *Exp. Brain Res.* 46:73–84. http://dx.doi.org/10.1007/BF00238100

Dix, J.A., and A.S. Verkman. 2008. Crowding effects on diffusion in solutions and cells. *Annu Rev Biophys.* 37:247–263. http://dx.doi.org/10.1146/annurev.biophys.37.032807.125824

Djukic, B., K.B. Casper, B.D. Philpot, L.S. Chin, and K.D. McCarthy. 2007. Conditional knock-out of Kir4.1 leads to glial membrane depolarization, inhibition of potassium and glutamate uptake, and enhanced short-term synaptic potentiation. *J. Neurosci.* 27:11354–11365. http://dx.doi.org/10.1523/JNEUROSCI.0723-07.2007

Eid, T., T.S. Lee, M.J. Thomas, M. Amiry-Moghaddam, L.P. Bjørnsen, D.D. Spencer, P. Agre, O.P. Ottersen, and N.C. de Lanerolle. 2005. Loss of perivascular aquaporin 4 may underlie deficient water and K^{+} homeostasis in the human epileptogenic hippocampus. *Proc. Natl. Acad. Sci. USA.* 102:1193–1198. http://dx.doi.org/10.1073/pnas.0409308102

Eilert-Olsen, M., N.N. Haj-Yasein, G.F. Vindedal, R. Enger, G.A. Gundersen, E.H. Hoddevik, P.H. Petersen, F.M. Haug, O. Skare, M.E. Adams, et al. 2012. Deletion of aquaporin-4 changes the perivascular glial protein scaffold without disrupting the brain endothelial barrier. *Glia.* 60:432–440. http://dx.doi.org/10.1002/glia.22277

Fenstermacher, J., and T. Kaye. 1988. Drug "diffusion" within the brain. *Ann. N. Y. Acad. Sci.* 531:29–39. http://dx.doi.org/10.1111/j.1749-6632.1988.tb31809.x

Frigeri, A., M.A. Gropper, C.W. Turck, and A.S. Verkman. 1995. Immunolocalization of the mercurial-insensitive water channel and glycerol intrinsic protein in epithelial cell plasma membranes. *Proc. Natl. Acad. Sci. USA.* 92:4328–4331. http://dx.doi.org/10.1073/pnas.92.10.4328

Grisar, T. 1984. Glial and neuronal Na^{+}-K^{+} pump in epilepsy. *Ann. Neurol.* 16(Suppl):S128–S134. http://dx.doi.org/10.1002/ana.410160719

Haj-Yasein, N.N., V. Jensen, G.F. Vindedal, G.A. Gundersen, A. Klungland, O.P. Ottersen, O. Hvalby, and E.A. Nagelhus. 2011a. Evidence that compromised K^{+} spatial buffering contributes to the epileptogenic effect of mutations in the human Kir4.1 gene (KCNJ10). *Glia.* 59:1635–1642. http://dx.doi.org/10.1002/glia.21205

Haj-Yasein, N.N., G.F. Vindedal, M. Eilert-Olsen, G.A. Gundersen, O. Skare, P. Laake, A. Klungland, A.E. Thorén, J.M. Burkhardt, O.P. Ottersen, and E.A. Nagelhus. 2011b. Glial-conditional deletion of aquaporin-4 (Aqp4) reduces blood-brain water uptake and confers barrier function on perivascular astrocyte endfeet.

Proc. Natl. Acad. Sci. USA. 108:17815–17820. http://dx.doi.org/10.1073/pnas.1110655108

Haj-Yasein, N.N., V. Jensen, I. Østby, S.W. Omholt, J. Voipio, K. Kaila, O.P. Ottersen, O. Hvalby, and E.A. Nagelhus. 2012. Aquaporin-4 regulates extracellular space volume dynamics during high-frequency synaptic stimulation: a gene deletion study in mouse hippocampus. *Glia.* 60:867–874. http://dx.doi.org/10.1002/glia.22319

Jauch, R., O. Windmüller, T.N. Lehmann, U. Heinemann, and S. Gabriel. 2002. Effects of barium, furosemide, ouabaine and 4,4′-diisothiocyanatostilbene-2,2′-disulfonic acid (DIDS) on iono-phoretically-induced changes in extracellular potassium concentration in hippocampal slices from rats and from patients with epilepsy. *Brain Res.* 925:18–27. http://dx.doi.org/10.1016/S0006-8993(01)03254-1

Li, J., and A.S. Verkman. 2001. Impaired hearing in mice lacking aquaporin-4 water channels. *J. Biol. Chem.* 276:31233–31237. http://dx.doi.org/10.1074/jbc.M104368200

Li, J., R.V. Patil, and A.S. Verkman. 2002. Mildly abnormal retinal function in transgenic mice without Müller cell aquaporin-4 water channels. *Invest. Ophthalmol. Vis. Sci.* 43:573–579.

Lu, D.C., H. Zhang, Z. Zador, and A.S. Verkman. 2008. Impaired olfaction in mice lacking aquaporin-4 water channels. *FASEB J.* 22:3216–3223. http://dx.doi.org/10.1096/fj.07-104836

MacVicar, B.A., D. Feighan, A. Brown, and B. Ransom. 2002. Intrinsic optical signals in the rat optic nerve: role for K$^+$ uptake via NKCC1 and swelling of astrocytes. *Glia.* 37:114–123. http://dx.doi.org/10.1002/glia.10023

Manley, G.T., M. Fujimura, T. Ma, N. Noshita, F. Filiz, A.W. Bollen, P. Chan, and A.S. Verkman. 2000. Aquaporin-4 deletion in mice reduces brain edema after acute water intoxication and ischemic stroke. *Nat. Med.* 6:159–163. http://dx.doi.org/10.1038/72256

Meeks, J.P., and S. Mennerick. 2007. Astrocyte membrane responses and potassium accumulation during neuronal activity. *Hippocampus.* 17:1100–1108. http://dx.doi.org/10.1002/hipo.20344

Nagelhus, E.A., Y. Horio, A. Inanobe, A. Fujita, F.M. Haug, S. Nielsen, Y. Kurachi, and O.P. Ottersen. 1999. Immunogold evidence suggests that coupling of K+ siphoning and water transport in rat retinal Müller cells is mediated by a coenrichment of Kir4.1 and AQP4 in specific membrane domains. *Glia.* 26:47–54. http://dx.doi.org/10.1002/(SICI)1098-1136(199903)26:1<47::AID-GLIA5>3.0.CO;2-5

Nagelhus, E.A., T.M. Mathiisen, and O.P. Ottersen. 2004. Aquaporin-4 in the central nervous system: cellular and subcellular distribution and coexpression with KIR4.1. *Neuroscience.* 129:905–913. http://dx.doi.org/10.1016/j.neuroscience.2004.08.053

Nicholson, C., and E. Syková. 1998. Extracellular space structure revealed by diffusion analysis. *Trends Neurosci.* 21:207–215. http://dx.doi.org/10.1016/S0166-2236(98)01261-2

Nielsen, S., E.A. Nagelhus, M. Amiry-Moghaddam, C. Bourque, P. Agre, and O.P. Ottersen. 1997. Specialized membrane domains for water transport in glial cells: high-resolution immunogold cytochemistry of aquaporin-4 in rat brain. *J. Neurosci.* 17:171–180.

Odette, L.L., and E.A. Newman. 1988. Model of potassium dynamics in the central nervous system. *Glia.* 1:198–210. http://dx.doi.org/10.1002/glia.440010305

Østby, I., L. Øyehaug, G.T. Einevoll, E.A. Nagelhus, E. Plahte, T. Zeuthen, C.M. Lloyd, O.P. Ottersen, and S.W. Omholt. 2009. Astrocytic mechanisms explaining neural-activity-induced shrinkage of extraneuronal space. *PLOS Comput. Biol.* 5:e1000272. http://dx.doi.org/10.1371/journal.pcbi.1000272

Padmawar, P., X. Yao, O. Bloch, G.T. Manley, and A.S. Verkman. 2005. K$^+$ waves in brain cortex visualized using a long-wavelength K$^+$-sensing fluorescent indicator. *Nat. Methods.* 2:825–827. http://dx.doi.org/10.1038/nmeth801

Papadopoulos, M.C., G.T. Manley, S. Krishna, and A.S. Verkman. 2004. Aquaporin-4 facilitates reabsorption of excess fluid in vasogenic brain edema. *FASEB J.* 18:1291–1293.

Ransom, B.R., C.L. Yamate, and B.W. Connors. 1985. Activity-dependent shrinkage of extracellular space in rat optic nerve: a developmental study. *J. Neurosci.* 5:532–535.

Ransom, C.B., B.R. Ransom, and H. Sontheimer. 2000. Activity-dependent extracellular K$^+$ accumulation in rat optic nerve: the role of glial and axonal Na$^+$ pumps. *J. Physiol.* 522:427–442. http://dx.doi.org/10.1111/j.1469-7793.2000.00427.x

Ruiz-Ederra, J., H. Zhang, and A.S. Verkman. 2007. Evidence against functional interaction between aquaporin-4 water channels and Kir4.1 potassium channels in retinal Müller cells. *J. Biol. Chem.* 282:21866–21872. http://dx.doi.org/10.1074/jbc.M703236200

Saadoun, S., M.C. Papadopoulos, H. Watanabe, D. Yan, G.T. Manley, and A.S. Verkman. 2005. Involvement of aquaporin-4 in astroglial cell migration and glial scar formation. *J. Cell Sci.* 118:5691–5698. http://dx.doi.org/10.1242/jcs.02680

Sick, T.J., E.L. Solow, and E.L. Roberts Jr. 1987. Extracellular potassium ion activity and electrophysiology in the hippocampal slice: paradoxical recovery of synaptic transmission during anoxia. *Brain Res.* 418:227–234. http://dx.doi.org/10.1016/0006-8993(87)90090-4

Solenov, E., H. Watanabe, G.T. Manley, and A.S. Verkman. 2004. Sevenfold-reduced osmotic water permeability in primary astrocyte cultures from AQP-4-deficient mice, measured by a fluorescence quenching method. *Am. J. Physiol. Cell Physiol.* 286:C426–C432. http://dx.doi.org/10.1152/ajpcell.00298.2003

Somjen, G.G. 1979. Extracellular potassium in the mammalian central nervous system. *Annu. Rev. Physiol.* 41:159–177. http://dx.doi.org/10.1146/annurev.ph.41.030179.001111

Strohschein, S., K. Hüttmann, S. Gabriel, D.K. Binder, U. Heinemann, and C. Steinhäuser. 2011. Impact of aquaporin-4 channels on K$^+$ buffering and gap junction coupling in the hippocampus. *Glia.* 59:973–980. http://dx.doi.org/10.1002/glia.21169

Su, G., D.B. Kintner, M. Flagella, G.E. Shull, and D. Sun. 2002. Astrocytes from Na$^+$-K$^+$-Cl$^-$ cotransporter-null mice exhibit absence of swelling and decrease in EAA release. *Am. J. Physiol. Cell Physiol.* 282:C1147–C1160.

Syková, E., and C. Nicholson. 2008. Diffusion in brain extracellular space. *Physiol. Rev.* 88:1277–1340. http://dx.doi.org/10.1152/physrev.00027.2007

Takumi, Y., E.A. Nagelhus, J. Eidet, A. Matsubara, S. Usami, H. Shinkawa, S. Nielsen, and O.P. Ottersen. 1998. Select types of supporting cell in the inner ear express aquaporin-4 water channel protein. *Eur. J. Neurosci.* 10:3584–3595. http://dx.doi.org/10.1046/j.1460-9568.1998.00360.x

Thiagarajah, J.R., M.C. Papadopoulos, and A.S. Verkman. 2005. Noninvasive early detection of brain edema in mice by near-infrared light scattering. *J. Neurosci. Res.* 80:293–299. http://dx.doi.org/10.1002/jnr.20439

Truc, O., J.P. Ollivier, and L.O. Nilsson. 2000. Numerical simulation of multi-species diffusion. *Materials and Structures.* 33:566–573. http://dx.doi.org/10.1007/BF02480537

Verkman, A.S. 2012. Aquaporins in clinical medicine. *Annu. Rev. Med.* 63:303–316. http://dx.doi.org/10.1146/annurev-med-043010-193843

Verkman, A.S., J. Ratelade, A. Rossi, H. Zhang, and L. Tradtrantip. 2011. Aquaporin-4: orthogonal array assembly, CNS functions, and role in neuromyelitis optica. *Acta Pharmacol. Sin.* 32:702–710. http://dx.doi.org/10.1038/aps.2011.27

Walz, W., and L. Hertz. 1982. Ouabain-sensitive and ouabain-resistant net uptake of potassium into astrocytes and neurons

in primary cultures. *J. Neurochem.* 39:70–77. http://dx.doi.org/10.1111/j.1471-4159.1982.tb04702.x

Walz, W., and L. Hertz. 1983. Intracellular ion changes of astrocytes in response to extracellular potassium. *J. Neurosci. Res.* 10:411–423. http://dx.doi.org/10.1002/jnr.490100408

Walz, W., and E.C. Hinks. 1985. Carrier-mediated KCl accumulation accompanied by water movements is involved in the control of physiological K$^+$ levels by astrocytes. *Brain Res.* 343:44–51. http://dx.doi.org/10.1016/0006-8993(85)91156-4

Xu, X., and C.J. Karwoski. 1994. Current source density analysis of retinal field potentials. II. Pharmacological analysis of the b-wave and M-wave. *J. Neurophysiol.* 72:96–105.

Yao, X., S. Hrabetová, C. Nicholson, and G.T. Manley. 2008. Aquaporin-4-deficient mice have increased extracellular space without tortuosity change. *J. Neurosci.* 28:5460–5464. http://dx.doi.org/10.1523/JNEUROSCI.0257-08.2008

Zador, Z., M. Magzoub, S. Jin, G.T. Manley, M.C. Papadopoulos, and A.S. Verkman. 2008. Microfiberoptic fluorescence photobleaching reveals size-dependent macromolecule diffusion in extracellular space deep in brain. *FASEB J.* 22:870–879. http://dx.doi.org/10.1096/fj.07-9468com

Zeng, X.N., X.L. Sun, L. Gao, Y. Fan, J.H. Ding, and G. Hu. 2007. Aquaporin-4 deficiency down-regulates glutamate uptake and GLT-1 expression in astrocytes. *Mol. Cell. Neurosci.* 34:34–39. http://dx.doi.org/10.1016/j.mcn.2006.09.008

Zhang, H., and A.S. Verkman. 2008. Aquaporin-4 independent Kir4.1 K$^+$ channel function in brain glial cells. *Mol. Cell. Neurosci.* 37:1–10. http://dx.doi.org/10.1016/j.mcn.2007.08.007

Zhang, H., and A.S. Verkman. 2010. Microfiberoptic measurement of extracellular space volume in brain and tumor slices based on fluorescent dye partitioning. *Biophys. J.* 99:1284–1291. http://dx.doi.org/10.1016/j.bpj.2010.06.023